Differential scanning calorimetry study of diffusional and martensitic phase transformations in some 9 wt-%Cr low carbon ferritic steels

Article *in* Materials Science and Technology · February 2011

DOI: 10.1179/026708309X12506933873260

CITATIONS
58

READS
388

7 authors, including:

Subramanian Raju
Indira Gandhi Centre for Atomic Research
95 PUBLICATIONS **732** CITATIONS
SEE PROFILE

Arun Kumar Rai
Raja Ramanna Centre for Advanced Technology
60 PUBLICATIONS **579** CITATIONS
SEE PROFILE

Eladath Mohandas
Indira Gandhi Centre for Atomic Research
153 PUBLICATIONS **2,175** CITATIONS
SEE PROFILE

M. Vijayalakshmi
Srimad Andavan Arts & Science College
165 PUBLICATIONS **2,164** CITATIONS
SEE PROFILE

Differential scanning calorimetry study of diffusional and martensitic phase transformations in some 9 wt-%Cr low carbon ferritic steels

B. Jeya Ganesh, S. Raju*, Arun Kumar Rai, E. Mohandas, M. Vijayalakshmi, K. B. S. Rao and Baldev Raj

The results of a comprehensive characterisation study of different phase transformations that take place upon heating and cooling in some low carbon, 9 wt-%Cr steels with varying concentrations of microalloying additions are presented in this paper. The steels investigated include: standard 9Cr–1Mo grade, V and Nb added modified 9Cr variety, controlled silicon added versions of plain 9Cr variety, (Ni + Mn) content controlled modified 9Cr welding consumables and one composition of W, Ta added reduced activation steel. The various on-heating diffusional phase changes up to the melting range and subsequent rapid cooling induced martensitic transformations are investigated in a controlled manner using differential scanning calorimetry under different heating and cooling rates, in the range 1–100 K min^{-1}. In addition to the accurate determination of Ac_1, Ac_3, $M_{23}C_6$, MX carbide dissolution and δ-ferrite formation temperatures upon heating, the melting range and the associated fusion enthalpy have also been established for these steels. The effect of prolonged thermal aging at temperatures of 823–873 K on austenite formation characteristics has also been investigated for standard and modified 9Cr–1Mo steels. The critical cooling rate for the formation of martensite on cooling from single phase austenite region is estimated to be about 4–5 K min^{-1} for all 9Cr steels investigated in this study. The effect of holding at 1273 K in the austenite region on martensite start temperature M_s, has also been evaluated as a part of this study. The experimental results are discussed in the light of the prevailing understanding of the physical metallurgy of high chromium low carbon steels.

Keywords: 9Cr steel, Phase transformation, Calorimetry, Microstructure, Martensite, Enthalpy

Introduction

It is well known that low carbon, highly alloyed ferritic–martensitic steels containing about 9 to 12 wt-%Cr with 0·1 to 0·15 wt-%C, and other controlled alloying additions, such as Mo, Mn, Nb, V, Si, W, Ta, Ni, Al, Cu, Co, N, B, etc., find their major application in conventional and nuclear power plants.[1–6] These steels possess good high temperature oxidation resistance,[7] higher values of thermal conductivity and lower thermal expansion coefficients[8] than the corresponding high strength austenitic stainless steels. Besides, the ferritic steels also have good tensile and creep rupture strength up to about 873 K,[9,10] in addition to fairly adequate welding characteristics[11] and fracture toughness properties[12] under typical power plant service conditions. Besides such general power plant related relevance, certain special grades of 9Cr based ferritic–martensitic steels, with carefully tailored minor element composition and heat treatment schedules are also the candidate materials for select fast fission and fusion reactor applications.[13,14] This nuclear relevance of 9Cr ferritic steels originates in their excellent swell resistance against high energy neutron irradiation.[15] In view of such wide spread application potential, it is only natural that many issues pertaining to physical, mechanical and process metallurgical aspects of these high chromium ferritic steels have drawn extensive attention in the past.[1,6] In fact, the research on the development of high temperature creep damage tolerant power plant ferritic alloys is still witnessing an active growth phase, as newer variants with adroitly engineered composition and processing controls are designed[16,17] to meet stiffer targets that are currently set with respect to operating temperature, stress and radiation levels, besides load following requirements.

Metallurgy and Materials Group, Indira Gandhi Centre for Atomic Research (IGCAR), Kalpakkam 603 102, Tamil Nadu, India

*Corresponding author, email sraju@igcar.gov.in

Published by Maney on behalf of the Institute
Received 25 June 2009; accepted 27 July 2009
DOI 10.1179/026708309X12506933873260

Added to their outstanding commercial appeal, ferritic steels also offer an interesting playground for conducting some fundamental investigations on alloy phase stability and phase transformation phenomena in ferrous systems. It is generally the case with ferritic alloys that they exhibit a spectrum of microstructural features which ensue as a consequence of different diffusional and displacive phase transformations that these steels experience during different processing steps. A fundamental understanding of the physical chemistry of these phase changes is therefore essential from the standpoint of enabling a systematic and knowledge driven approach to the design of service stable microstructure in these alloys.[18] Despite the fact that quite an extensive information based on microstructure–property–performance correlation has already been built up over the years for the power plant steels,[6,19–21] there is nevertheless a paucity of reliable data on basic thermodynamic and kinetic quantities associated with diffusional and martensitic phase transformations. In particular, accurate experimental data on transformation temperatures, their dependence on thermal history, the enthalpy values associated with different phase changes and the transformation kinetic parameters such as diffusional mobility and activation energy, etc., are still not available in open literature for many advanced 9Cr steels. It is amidst this background that the authors have initiated in the recent past, a comprehensive calorimetry based characterisation of thermodynamic and kinetic facets of phase changes that are generic to low carbon high chromium nuclear grade ferritic steels. As a part of this broad based research initiative, an attempt has been made in this study to measure accurately the phase transformation characteristics in ten typical alloy compositions belonging specifically to low carbon 9Cr based ferritic steel family. It may be added that these compositions are of special interest to Indian Fast Reactor program, in the sense that specific compositional adjustment of the standard commercial varieties, such as EM10 and P/T91 has been done to suit our indigenous design stipulations of select in pile and out of pile applications in sodium cooled fast reactors and also as a prospective candidate material for certain fusion related applications.

The primary experimental technique adopted in the present study is differential scanning calorimetry (DSC), in which appropriate standards have been employed for accurate temperature and heat flow calibration. Further by imposing precisely controlled heating, isothermal holding and cooling schedules on well characterised small and regularly shaped samples, it is in principle possible to study the phase transformation phenomenon with minimal problems arising from internal thermal gradients and large instrumental thermal lag.[22] Taking adequate care of these issues facilitates obtaining reliable transformation temperature data using thermal analysis techniques.[23] To begin with, the relevant experimental details are presented briefly in the following section.

Experimental details

Composition, heat treatment and general metallographic characterisation

In Table 1, the chemical compositions in weight percentage of different 9Cr steels investigated in this

Table 1 Chemical composition different 9Cr based ferritic–martensitic steels investigated in this study, wt-%

Composition, wt-%																						
Steel designation number	Details	C	Cr	Mo	Mn	Si	V	Al	Ni	P	Co	Cu	Sn	S	N	W	Ti	Nb	Ta
Plain 9Cr–1Mo steel																			
1	Plain 9Cr–1Mo	0·1	8·44	0·94	0·46	0·49	0·001	0·011	0·17	0·008	…	0·11	…	0·002	0·008	…	…	…	…
Silicon added plain 9Cr–1Mo steel																			
2	9Cr–1Mo–0·24Si	<0·07	9	1·00	0·53	0·24	0·024	0·055	<0·1	<0·007	<0·009	<0·05	<0·008	<0·007	…	…	…	…	…
3	9Cr–1Mo–0·42Si	0·074	9	0·96	0·41	0·42	0·025	0·021	<0·1	<0·007	<0·009	<0·05	<0·008	<0·007	…	…	…	…	…
4	9Cr–1Mo–0·60Si	0·073	8·58	0·94	<0·3	0·6	0·022	0·058	<0·1	<0·007	<0·009	<0·05	<0·008	<0·007	…	…	…	…	…
Mod. 9Cr–1Mo and its welding consumables																			
5	Mod. 9Cr–1Mo	0·097	8·29	0·92	0·37	0·31	0·26	0·006	0·38	0·018	…	…	…	0·0047	0·057	…	…	0·08	…
6	Welding consumable 1	0·06	9·24	1·05	1·37	0·3	0·17	…	0·95	0·005	…	…	…	0·001	0·03	…	…	0·03	…
7	Welding consumable 2	0·075	9·3	1·00	1·2	0·3	0·23	…	0·65	0·008	…	…	…	0·007	0·04	…	…	…	…
8	Welding consumable 3	0·1	9	0·99	1	0·24	0·17	<0·01	0·7	0·009	…	<0·05	…	0·012	0·055	…	…	0·009	…
9	Welding consumable 4	0·084	8·89	0·93	0·6	0·3	0·22	…	0·75	0·007	…	…	…	0·0034	0·0375	…	…	0·05	…
10	Typical base metal	0·097	9·29	0·92	0·37	0·31	0·26	…	0·38	0·018	…	…	…	0·0047	0·057	…	…	0·08	…
Reduced activation ferritic–martensitic steel																			
11	Reduced activation steel (RAFM)	0·091	9·05	0·0036	0·56	0·05	0·226	0·0036	…	…	0·0043	0·005	…	…	0·0206	1	0·0024	0·0039	0·063

study are listed. It is clear that all the steels listed in Table 1, despite belonging to the same basic category, have certain compositional differences with respect to some minor alloying additions. In order to bring out this fact rather explicitly, the steels are grouped into following categories:

(i) standard or plain 9Cr–1Mo–0·1C variety
(ii) silicon added plain 9Cr steels
(iii) modified 9Cr–1Mo steel containing controlled V, Nb addition
(iv) welding consumables designed for modified 9Cr–1Mo steels with adjusted Mn + Ni content
(v) W and Ta substituted reduced activation ferritic–martensitic (RAFM) steel

At the outset, it must be mentioned that these compositions are not specifically designed with a view to isolate and study the effect of one or a few select minor alloying additions on transformation characteristics. On the contrary, each one of these alloys were melted at different times to suit the then emerging design specifications for different applications in sodium cooled fast reactors. In the present study, an attempt is made to gather accurate data on transformation temperatures on these assorted compositions and compare the results in the light of prevailing scenario on the physical metallurgy of high chromium ferritic steels.

In general, these alloys are made by repeated vacuum induction melting followed by vacuum arc refining. The ingots are shaped into plate forms by hot forging and rolling with a finish temperature of about 1273 K. The plates are aircooled to room temperature subsequently. The different steel plates are generally supplied in the normalised and tempered (N&T) condition (refer to Table 2, for heat treatment details). This generic heat treatment refers to slow heating of a steel plate to a temperature of about 1253 to 1323 K depending on the actual composition. This is followed by an isothermal hold of about 30 min at this temperature, after which the samples are air cooled or at times water quenched to room temperature. The air cooling treatment goes by the name of normalisation, which in 9Cr steels generally yields about 100 % martensite, with of course slightly varying hardness values depending on the composition. The normalised steels are subsequently tempered at 1033–1053 K for varying time durations. Since the transformation characteristics of ferritic–martensitic steels are known to be sensitive to the starting microstructure,[24] an attempt has been made to produce slightly different initial microstructure conditions by aging the normalised and tempered (N&T) structure to varying time durations. The actual details concerning heat treatment are presented in Table 2. It must also be added that bulk of the heat treatment is carried out in air on plate samples. However, a few select treatments with regard to studying the martensitic transformation are carried out *in situ* in DSC, under highly pure argon (99. 999 mass per cent) atmosphere.

A representative slice from the given steel plate is used for standard metallographic examination and X-ray diffraction characterisation after due sample preparation.

Table 2 Heat treatment details adopted for each steel composition and corresponding lattice parameter for α-ferrite phase and Vickers microhardness number are tabulated

Steel designation number	Heat treatment	α-ferrite lattice parameter, nm	Average microhardness number, (VHN)
1a	Plain 9Cr–1Mo quenched from 1323 K to room temperature (RT)	0·2874	464
1b	Plain 9Cr–1Mo N&T 1323 K/15 min + 1033 K/2 h	0·2875	274
1c	Plain 9Cr–1Mo N&T and aged 823 K/500 h	0·2870	254
1d	Plain 9Cr–1Mo N&T and aged 823 K/5000 h	0·2873	274
1e	Plain 9Cr–1Mo N&T and aged 923 K/500 h	0·2871	287
2	Si added 9Cr–1Mo N&T 1253 K/30 min + 1023 K/30 min	0·2874	233
3	Si added 9Cr–1Mo N&T	0·2873	236
4	Si added 9Cr–1Mo N&T	0·2875	245
5a	Mod. 9Cr–1Mo N&T 1323 K/15 min + 1033 K/2 h	…	248
5b	Mod. 9Cr–1Mo N&T and aged 773 K/10 000 h	…	294
5c	Mod. 9Cr–1Mo N&T and aged 823 K/10 000 h	…	300
5d	Mod. 9Cr–1Mo N&T and aged 873 K/10 000 h	…	286
5e	Mod. 9Cr–1Mo N&T and aged 773 K/20 000 h	…	299
5f	Mod. 9Cr–1Mo aged 823 K/20 000 h	…	293
5g	Mod. 9Cr–1Mo N&T and aged 873 K/20 000 h	…	286
6	Mod. 9Cr weld consumables TIG weld pad	0·2876	485
7	Weld pad	0·2875	487
8	Weld pad	0·2876	514
9	Filler wire	0·2872	556
10	Base metal	0·2873	341
11a	Reduced activation steel as received hot rolled at 1273 K; air cooled to RT	0·2877	497
11b	Reduced activation steel 1253 K/2 h/air cooled	…	429
11c	Reduced activation steel 1453 K/2 h/air cooled	…	435
11d	Reduced activation steel 1453 K/water cooled	…	482
11e	Reduced activation steel 1553 K/water cooled	…	427
11f	Reduced activation steel 1553 K/furnace cooled	…	232
11g	Reduced activation steel N& T 1253 K/air cooled/1053 K/2 h	…	207
11h	Reduced activation steel N& T 1253 K/air cooled/1053 K/5 h	…	195

For light microscopy observation, the final polished samples are given a mild initial etch with 2% nital solution, followed by swabbing with Vilella's reagent. The metallographic observation has been carried out using a Leica-MeF4A optical microscope and the X-ray studies using an INEL powder diffractometer. The hardness measurements have been made using a Leitz microhardness tester under a load of 100 g. A total of about eight to ten hardness readings are recorded on each sample and the average value is reported here.

Differential scanning calorimetry (DSC) experiments

The DSC studies have been performed using Setaram Setsys 16 high temperature heat flux type differential scanning calorimeter. The instrumental details are elaborated in our previous publications[24,25] and only the major points are highlighted here. The calorimeter consists of a DSC cradle or plate that is vertically suspended from the top support structure through a guiding annular alumina tube. The DSC plate itself is a thin rectangular constantan strip with provisions for safely accommodating two small 100 μL volume identical recrystallised alumina crucibles on its either side. One of these crucibles is kept empty, while the other houses the sample. The presence of a thin platinum strip connecting these two crucibles serves the purpose of the thermal resistor that transports the heat flux generated in one of the crucibles to the other one. The temperatures of the empty crucible and the one containing sample are monitored by B type (Pt–Pt/Rh) thermocouple that is housed exactly beneath the DSC cradle with less than 2 mm gap. The suspended DSC cradle together with the thermocouple sensor constitutes the DSC probe, which is housed inside the well equilibrated constant temperature zone of argon cover gas filled and water cooled graphite furnace.

In DSC experiments, small, well cleaned samples of mass varying from 40 to 70 mg are used. These are cut from the originally supplied plate using a diamond coated slow speed wire saw. The specimen chamber of DSC is alternately evacuated and purged with high pure argon (Iolar grade, 99·999% purity) a few times, before the commencement of an experimental run. A steady argon flow of about 50 mL min^{-1} is maintained through out the experiment and an argon pressure of about 1000–1300 mbar is maintained in the graphite furnace chamber to avoid oxidation during prolonged holds at high temperatures. A typical DSC experimental run employed in the present study consists of following heating and cooling schedules:

(i) to begin with, the furnace temperature is gradually raised to 373 K at the rate of about 10 K min^{-1} and is allowed to stabilise at this temperature for about 15 min. This preconditioning minimises the thermal gradient in the sample and facilitates the attainment of a smooth baseline. This is followed by the actual heating ramps and holding isotherms that are characteristic of the present continuous heating DSC experiments

(ii) in an actual experimental run, the sample is heated at a predetermined rate from 373 to 1833 K or to 1523 K in some runs and is equilibrated at this temperature for about 15 min, and then cooled at the same rate to 373 K, again kept at this temperature for a period of about 15 min, before finally cooling to room temperature. The scanning rate employed varied between 1 to 3 K min^{-1} for those experiments in which the sample is taken up to the melting regime. In this set of slow heating experiment, the thermal lag and thermal gradient are minimal and it is believed that various on-heating transformation arrest points are recorded under close to equilibrium conditions.

In the second set of experimental runs, which are conducted to record the variations in lower (Ac_1) and upper (Ac_3) critical transformation temperatures with thermal history, different rates of heating and cooling in the range 1 to 100 K min^{-1} are adopted. The maximum temperature in these latter set of experiments is restricted to 1273–1473 K only, which is adequate for the realisation of complete carbide dissolution and ensuring a fully austenitic single phase in 9Cr steels.[26] Fresh samples are employed for each individual experiment, and a few repeat runs were also performed on select steels to assess the reproducibility of transformation temperatures. In the present study, the transformation temperatures are reproducible to $\pm 2\%$ for slow to moderate heating rates of about 40 K min^{-1}.

(iii) the base line calibration runs have been performed for each scan rate under identical experimental heating and cooling conditions using the *same* pair of empty crucibles on both sides of the DSC cradle. The temperature calibration has been done using the melting points of pure aluminium, zinc, tin, copper, silver, gold and Armco iron standards. The heat flow calibration is done in terms of the polymorphic transitions in pure iron (Aldrich Chemicals) with 80 mass ppm of combined interstitial impurities. The presence of the invariable time lag between the actual temperature experienced by the sample and that imposed by the heating rate during the course of a phase transformation event has also been calibrated using pure iron signal as the reference. For the typical experimental conditions adopted in this study, such as the scan rates of 10 to 40 K min^{-1}, sample mass of about 50–75 mg, and with a argon flow rate of 50 mL min^{-1}, the time lag is found to be about 5 s (for the polymorphic transformation in iron). This translates roughly into ± 3 to 5 K uncertainty in the measured transformation temperatures, although a slightly lower uncertainty is recorded for slower heating rate 1–3 K min^{-1} experiment.

Results

General microstructure

In Fig. 1, the optical micrograph portraying the typical normalised and tempered microstructure of plain 9Cr–1Mo steel (steel no. 1 in Table 1) is presented. This microstructure is representative of the ones that are usually found in this class of steels.[18] The prior austenite grain size is found to vary in the range of 25–60 μm for 1253–1323 K/15–30 min solutionised samples. The typical microhardness values of the normalised and tempered microstructure are found to be of the order of 230–290 VHN. However, the martensitic microstructure

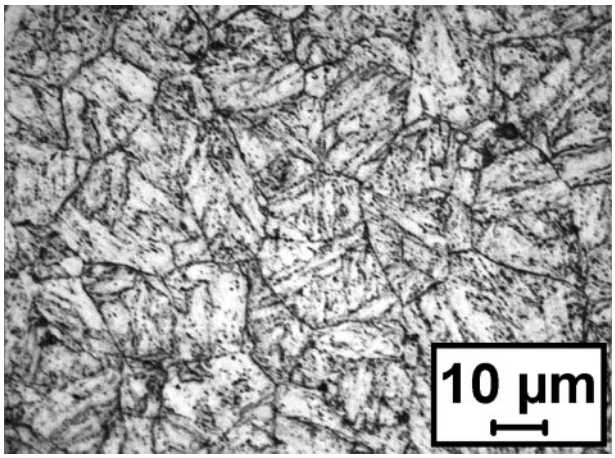

1 Typical normalised and tempered microstructure of tungsten added low carbon 9Cr steel

obtained after a direct normalising treatment exhibited a higher hardness value, exceeding about 400 VHN. The martensites obtained in the case of TIG weld deposits of modified 9Cr welding consumables which have higher (Ni+Mn) content than the rest of 9Cr steel compositions (Table 1) showed the highest hardness of about 550 VHN. Here the composition and high cooling rates experienced during welding have jointly enabled the formation of harder martensite.

As for the lattice parameter values of the α-ferrite phase in different compositions are concerned, not much variation is found (Table 2), although some marginal increase is noticed with respect to silicon enhancement in standard 9Cr variety (steel nos. 2–4 in Table 1) and also in W, Ta substituted reduced activation steel (steel no. 10 in Table 1). The hardness and lattice parameter data are summarised in Table 2.

Phase transformation sequence during heating

In Fig. 2*a*, a typical DSC thermogram obtained during slow heating to the melting region followed by similar slow cooling to room temperature, of a normalised plain 9Cr–1Mo steel (steel no. 1 in Table 1) is illustrated. The occurrence of different transformation events are indicated by arrows in Fig. 2*a*. In Fig. 2*b*, an expanded portrayal of the same curve around the melting region is shown. The plain 9Cr steel is taken here as an illustrative example to explain the typical sequence of various on-heating phase changes that are generic to high chromium steels. The transformation temperature data for other compositions are listed in Table 3. To begin with, the sequence of phase transformations that occur upon heating is taken up for a detailed enumeration.

Since the starting microstructure obtained after the normalising treatment is one of untempered martensite, the first shallow exothermic thermal arrest occurring around 873 K, corresponds to the onset of $M_{23}C_6$ carbide precipitation from carbon saturated martensite.[24,25] Although it is quite likely that the relaxation of the defect structure of martensite could well have been initiated at temperatures lower than 873 K, we could not detect this preprecipitation low temperature relaxation in the present study due to its weak heat flow effect.[24] The second thermal arrest recorded in this study is due to the ferromagnetic→paramagnetic transformation of the α-ferrite phase upon reaching T_C (arrow pointer

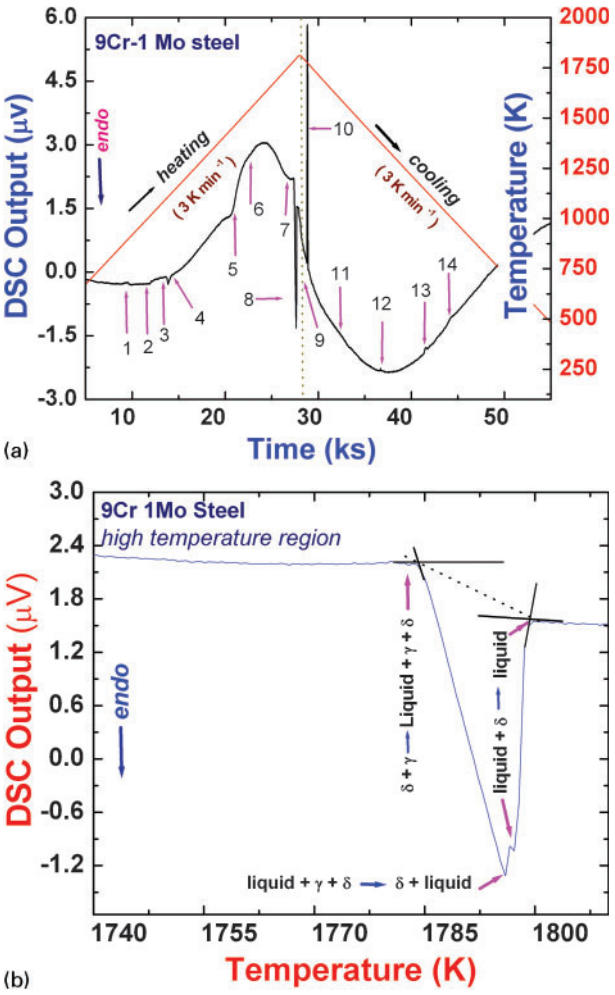

2 *a* typical DSC profile of normalised and tempered 9Cr–1Mo–0·1C steel obtained during slow heating to melting and subsequent cooling to room temperature. Different thermal arrests arising from phase transformation events are marked by arrows and *b* expanded view of DSC profile shown in Fig. 2*a* around melting region

no. 2), the Curie temperature.[25] The Curie temperature T_C, for plain 9Cr steel is found to be about 1014±3 K. Since the net magnetic moment or the effective magnetic interaction in α-ferrite is expected to be composition sensitive, it follows that T_C among the ferritic steel compositions studied here also reflects this composition dependence. As shown in Table 3, T_C is found to vary from 986 to 1018 K. The lowest T_C is recorded for the weld consumable with a comparatively high (Ni+Mn) content (steel no. 7 in Table 1), while slightly higher value is recorded for W, Ta containing reduced activation steel (steel no. 11 in Table 1). It must also be added as a general remark that addition of alloying elements other than Co to pure iron, serves to reduce its T_C. Thus, the measured values of T_C for different 9Cr steels are in accordance with general metal physics considerations.

The third clearly delineated endothermic peak arises from the γ-austenite formation from α-ferrite+$M_{23}C_6$ carbide. The onset of γ-austenite formation (arrow pointer no. 3) is conventionally designated as the Ac_1 temperature and the transformation off-set (arrow pointer no. 4) is denoted as Ac_3. Again for plain 9Cr steel, these temperatures are in the range 1093 and

1137 K respectively.[27] It must be said at this point that both Ac_1 and Ac_3 temperatures, as obtained in the present study are actually kinetic quantities, in the sense that they are dependent on thermal history.[28] Under true thermodynamic equilibrium conditions, the austenite formation and completion are supposed to be over at Ae_1 ($<Ac_1$) and Ae_3 ($<Ac_3$) temperatures respectively. Furthermore, according to equilibrium thermodynamic calculations, the completion of $M_{23}C_6$ dissolution in austenite is also supposed to be nearly complete at Ae_3, the equilibrium analogue of Ac_3.[29] But the operation of ubiquitous kinetic retardation effects associated with the carbide dissolution step in high chromium alloys[30–32] renders 100 % carbide dissolution only at a temperature higher than even Ac_3. As a result, it often is the case with highly alloyed ferritic steels, that the effective spread of the intercritical zone (Ac_3-Ac_1) is larger than its equilibrium value (Ae_3-Ae_1). This kinetics induced pseudo expansion of the intercritical domain featuring metastable ($\alpha+\gamma+$carbide) equilibrium is in fact more pronounced under rapid heating conditions.[33] This point will be discussed in detail at a latter instance in this paper. Now, reverting back to carbide dissolution step during heating, it may be said that this being a gradual or continuous process, a sharp thermal arrest is not witnessed in the standard DSC profile. In addition, the volume fraction of the carbide phase being small (less than 2–3%) in these alloys, the contribution to the overall enthalpy change arising from its dissolution is also a trifle as compared to the overall enthalpy change associated with $\alpha\rightarrow\gamma$ transformation. Because of these two facts, the $M_{23}C_6$ carbide dissolution upon heating can only be discerned as a broad endothermic trough in a suitably baseline compensated DSC profile. The transformation arrest (point no. 5) placed at 1483 K is thus taken to be associated with the formation of carbide free single phase austenite.

At still higher temperatures of about 1573 K, the formation of δ-ferrite from γ-austenite phase results, yielding ($\gamma+\delta$) two phase domain (arrow pointer no. 6). The ensuing three transformation arrest points marked as, 7, 8 and 9 in Fig. 2*a* are associated with the formation of the first trace of liquid at 1783 K and the subsequent complete dissolution of γ-austenite in liquid at 1796 K to yield the ($\delta+$L) two phase regime. The completion of melting is finally realised at 1797 K; pointer no. 9), which may be taken as the liquidus temperature for this steel under slow continuous heating conditions. The nature of the thermal arrest events associated with the high temperature phase changes is more clearly depicted in Fig. 2*b*.

As mentioned before, the above mentioned sequence of phase transformation events is generic to any 9Cr based low carbon steel. However, in certain grades like P/T91 or RAFM variety, in which controlled amounts of V and Nb,[1,2] or W, Ta in the case of reduced activation version,[34] are added to enhance the high temperature creep strength, the presence of strong carbide formers such as Nb, V and Ta results in the formation of MX type carbides and mixed carbonitrides, depending on the actual nitrogen content.[35] The solvus temperature of MX carbide or carbonitride is higher than that of cubic $M_{23}C_6$ carbide,[36] and hence in V, Nb, and Ta containing steels, there will be an additional reaction step associated with the dissolution of this NaCl type MX phase in austenite. In general terms, this additional thermal event, like its predecessor, namely the $M_{23}C_6$ dissolution reaction, is seldom clearly noticed in a thermal analysis profile due to its smaller enthalpy effect. It must also be added that the volume fraction of the MX phase is also smaller than that of $M_{23}C_6$. The clear detection of MX dissolution temperature is therefore a formidable task in DSC studies involving samples of low mass. In the present study, we have taken recourse to identifying this inflection point by going in for the derivative analysis of the base line subtracted DSC signal. The values of transformation temperatures thus obtained for different 9Cr steels are collected together in Table 3.

Diffusional phase changes observed during slow cooling

On cooling from the liquid state, the actual course of various phase changes occurring in a ferritic steel is decided by the cooling rate.[19] Since low carbon 9Cr steels are known for their high degree of hardenability,[4] even a fairly slow cooling rate like 5 K min^{-1} from single phase austenite domain is adequate for nucleating

Table 3 Tabulation of measured on-heating phase transformation temperatures for different ferritic steels listed in Table 1*

Description of phase change	Steel designation number in Table 1										
	1	2	3	4	5	6	7	8	9	10	11
	Transformation temperature, K										
α' (martensite)$\rightarrow\alpha$ (ferrite)$+M_{23}C_6$	873	888	881	885	897	930	947	937	944	903	937
T_C, Curie temperature	1041	1041	1011	1014	1016	1004	986	1013	1004	1012	1018
$\alpha+$(V,Nb)(C,N)$+M_{23}C_6\rightarrow\alpha+\gamma+$ (V,Nb)(C,N)$+M_{23}C_6$ (Ac_1)	1093	1112	1112	1134	1127	1072	1045	1080	1072	1102	1104
$\alpha+\gamma+$(V,Nb)(C,N)$+M_{23}C_6\rightarrow\gamma+$ (V,Nb)(C,N)$+M_{23}C_6$ (Ac_3)	1137	1133	1156	1166	1159	1120	1100	1117	1095	1138	1144
$\gamma+$(V,Nb)(C,N)$+M_{23}C_6\rightarrow\gamma+$(V,Nb)(C,N)	1483	1474	1473	1508	1513	1513	1522	1520	1543	1522	1550
$\gamma+$(V,Nb)(C,N)$\rightarrow\delta+\gamma+$(V,Nb)(C,N)	1573	1607	1617	1643	1553	1567	1583	1572	1598	1573	1585
$\delta+\gamma+$(V,Nb)(C,N)$\rightarrow\delta+\gamma$	…	…	…	…	1643	1632	1653	1599	1655	1659	1681
$\delta+\gamma\rightarrow$liquid$+\gamma+\delta$	1783	1790	1786	1785	1775	1793	1790	1795	1795	1793	1730
Liquid$+\gamma+\delta\rightarrow$liquid$+\delta$	1796	1799	1796	1795	1777	1796	1793	1796	1798	1794	1753
Liquid$+\delta\rightarrow$liquid	1797	1800	1799	1800	1796	1804	1800	1806	1806	1802	1805

*These values are obtained under slow heating rate of about 1–3 K min^{-1}. Note that in case of plain 9Cr steels the transformation temperature corresponding to the MX type carbide dissolution is absent. In case of reduced activation steel, the MX precipitate corresponds to (V,Ta)(C,N).

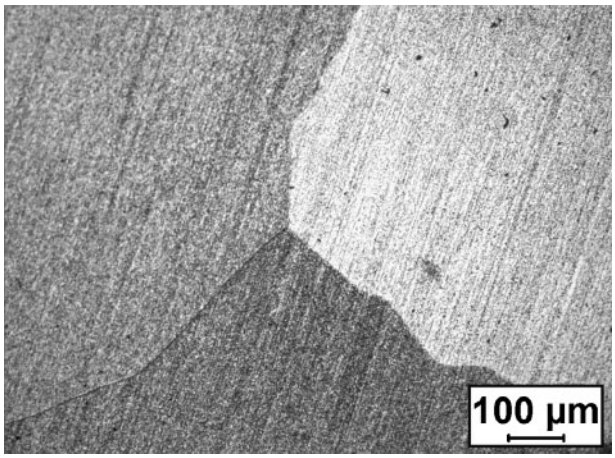

3 Microstructure of very slowly cooled (1 K min^{-1}) 9Cr–1Mo steel sample showing large grained alpha ferrite phase

the martensite. Therefore, in order to enforce the diffusional mode of austenite decomposition during cooling, we have adopted still lower cooling rates of about 1–3 K min^{-1}. A typical DSC thermogram obtained under such conditions is presented in the right half of Fig. 2*a*. From this figure, it is clear that a certain degree of asymmetry is present between heating and cooling part of the DSC profile, not withstanding the fact that identical scan rates are employed in both forward and reverse scans. The different transformation arrest events occurring during cooling are indicated by consecutively numbered arrow pointers, 11 to 14. The formation of the δ-ferrite phase from liquid (pointer 11), γ-austenite phase (pointer 12) and $M_{23}C_6$ precipitation (pointer 13) and the Curie point (pointer 14) are all fairly discernible. The microstructure of the slowly cooled sample (1 K min^{-1}) is shown in Fig. 3. The presence of large grained rather featureless α-ferrite phase with a hardness of about 150 VHN is readily seen in this micrograph. The diffusional phase changes during cooling are not discussed any more here and instead, the attention is focused on the martensitic mode of austenite decomposition on fast cooling.

Martensite formation on fast cooling

The formation of martensite from austenite is also readily witnessed in the DSC profile, provided the cooling rate from the single phase high temperature austenite exceeds a threshold value known as the critical cooling rate. In the present study, the critical cooling rate is estimated to be about 4–5 K min^{-1}. This critical cooling rate is determined in a separate set of experiments in which nearly identical samples, are heated depending on the steel composition to 1253–1373 K and kept at this temperature for about 15 min to ensure complete carbide dissolution and the consequent formation of homogeneous austenite. These samples are then cooled *in situ* in the DSC cell to room temperature at varying rates in the range, 1 to 100 K min^{-1}. The minimal cooling rate which yielded the first measurable trace of the exothermic signal associated with the formation of martensite (Fig. 4) is taken as the critical cooling rate. A typical exothermic thermal arrest associated with the martensite formation upon fast cooling is quite vividly revealed in the DSC profile, shown in Fig. 4.

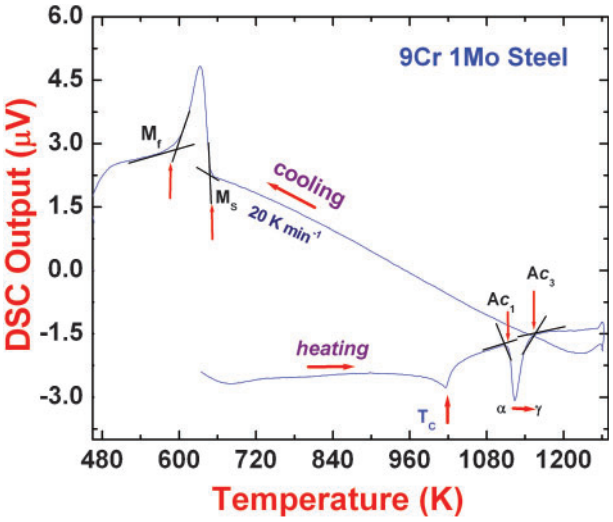

4 Profile (DSC) showing exothermic thermal arrest associated with formation of martensite upon cooling

In Fig. 5, the effect of increasing the cooling rate on the hardness of the transformation product is graphically illustrated for the tungsten added reduced activation steel (steel no. 10 in Table 1). This figure is quite typical of 9Cr steels investigated in this study. The emergence of two clearly delineated regions with respect to the transformation mode is clearly brought out by the hardness variation seen in this figure. For slow cooling (1–3 K min^{-1}), only the α-ferrite phase with a comparatively low hardness value (180 to 200 VHN) is obtained. It is only when the rate of cooling exceeds about 4 to 5 K min^{-1}, the formation of hard martensite phase is realised. The formation of martensite is attested by the marked rise in hardness of the quenched microstructure (Fig. 5). It is also clear from Fig. 5 that the hardness of the quenched

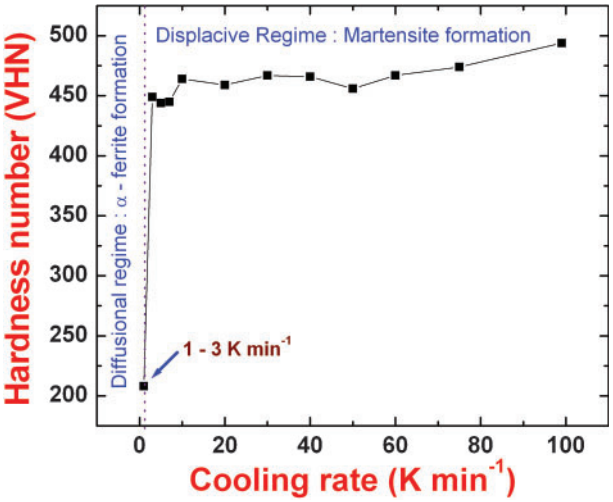

5 Effect of cooling rate from high temperature austenite region on hardness of transformation product. Note that for low cooling rates, only diffusional formation of α-ferrite with low hardness values is realised. However, martensite formation occurs for cooling rates exceeding about 5 K min^{-1}. Solutionising temperature in all these experiments is kept constant at 1273 K

martensite is somewhat insensitive to the increase in cooling rates in the initial region following just after the critical cooling rate; but with further progressive increase in the severity of cooling, the hardness curve shows an upward trend, which suggests that martensite which forms under higher cooling rates must possess higher defect density, and this in turn contributes to the higher strength of martensite. In addition, it is also found that for a fixed austenitising time of about 15 min, varying the solutionising temperature in the range 1253 to 1323 K did not produce significant changes in the martensite characteristics. However, prolonged holds of the order of 2 h and above, at a high enough austenitising temperature 1373 K resulted in an appreciable growth of austenite grain size, and this had a marked effect in changing the M_s temperature. This is especially found to be so in the case of tungsten and tantalum substituted reduced activation variety[37] in which the higher solutionising temperature and prolonged time holds accelerated the dissolution of carbide phases in austenite and thus affecting the austenite composition significantly. It is only obvious that a change in austenite composition affects the M_s temperature significantly.[38] In deference to the limited scope of this paper, a detailed discussion of the kinetic aspects of martensitic transformations in 9Cr steels is not presented here.[37]

In addition to measuring various transformation arrest temperatures, the authors have also determined in the present study both $\Delta^{\circ}H^{\alpha\rightarrow\gamma}$ and $\Delta^{\circ}H^{\gamma\rightarrow\alpha'}$, the transformation enthalpies associated with the diffusional α+carbides$\rightarrow\gamma$-austenite; and the displacive $\gamma\rightarrow\alpha'$-martensite, transformations respectively from the corresponding area under the transformation peak. These data are tabulated in Table 4. In addition, the authors have also estimated the solidus and liquidus temperatures associated with the melting phenomenon. It may be reiterated that the required calibration of the heat flow signal to obtain effective enthalpy is performed in terms of the reference signal obtained with a known mass of pure iron. It is estimated that the quoted enthalpy values in the present study are accurate to $\pm 5\%$.

One important point about the transformation temperatures determined by thermal analysis technique is that they are dependent on thermal history, in the sense that they exhibit appreciable heating or cooling rate dependence. This issue arises from the ubiquitous kinetic retardation of the actual progress of the diffusional phase changes under the influence of forced rapid change in the thermal field prevailing at the transformation front. Taking care to minimise the uncertainties arising from the instrumental thermal lag by proper calibration, the heating rate dependence of transformation temperatures can be quantitatively modelled to yield effective or apparent activation energy for the overall phase change.[39–41] This issue is not dealt with here in any detail considering the restricted scope of this paper. However, mention must be made of the fact that experiments are conducted for a series of heating and cooling rates to determine the corresponding variations in Ac_1, Ac_3, M_s and M_f temperatures. These are then extrapolated to hypothetical zero scan rate to effect a comparison with equilibrium thermodynamic estimates.

Discussion

General observations

In order to facilitate proper understanding of the temperature driven phase changes occurring in high chromium ferritic steels under equilibrium conditions, as shown in Fig. 6, a calculated vertical section or isopleth for the multicomponent 9Cr ferritic steel.[42] As may be seen from this equilibrium diagram, that for standard 9Cr steel with a low carbon content in the range 0·1 to 0·2 wt-%, the sequence of various on-heating phase changes observed in the present study is in good accord with the theoretical prediction. The actual values for the measured transformation temperatures do of course vary from the predicted ones, as they are influenced significantly by the starting microstructure and other kinetic factors. But notwithstanding this limitation, the agreement between the experimental and calculated transformation temperatures is indeed good.

Before proceeding to discuss the present results in the light of the information gleaned from literature, it may be remarked that to best of these authors knowledge, there is not much systematically generated and critically assessed experimental information on the transformation temperatures in high chromium ferritic steels, especially the influence of minor alloying additions. In fact, a literature search for possible comparison of the present experimental estimates of the melting temperature along with the melting enthalpy values for high chromium ferritic steels did not yield any fruitful result. In a similar vein, the thermodynamic and kinetic issues of martensitic transformation are also not critically dealt with in these technologically important materials. It appears that the work of Finkler and Schirra[43] on the determination of TTT and CCT diagrams for numerous ferritic steel compositions belonging to 8–14 wt-%Cr is the most comprehensive one to date, providing experimental data on isothermal and continuous cooling transformation diagrams and transformation temperatures such as Ac_1, Ac_3 and M_s. Since then, there has not been a renewed attempt at a similar scale to enlist the transformation characteristics of high chromium ferritic steels, notwithstanding a few discrete attempts on select compositions.[44–46] Thus for example, the on-heating austenite formation in few select 9Cr based reduced activation steels containing tungsten and tantalum has recently been investigated by Danon and Alamo using dilatometry.[46] However, in this investigation, information on transformation enthalpies and transformation arrest temperatures up to the melting region have not been gathered, as the maximum temperature of investigation is mostly restricted to the single phase austenite region only. In view of such lack of comprehensive experimental information, we could not make a critical appraisal of the data gathered in this study. Instead, what has been attempted is a logical analysis of the results in the light of the basic physical metallurgy of high chromium ferritic steels.

Trends in Ac_1, Ac_3 temperatures

For a given starting microstructure and thermal history, it is well known that the trend in austenite start temperature (Ac_1) during continuous heating is decided more by the composition, while the kinetic factors associated with the sluggish alloy carbide (rich in

Table 4 Listing of lower critical (Ac_1), upper critical (Ac_3) and martensitic start (M_s) transformation temperatures and enthalpies $\Delta^\circ H^{\alpha\rightarrow\gamma}$ and $\Delta^\circ H^{\gamma\rightarrow\alpha'}$ associated with the austenite formation and martensite transformation respectively for different steels with different starting microstructures*

Steel designation number	Heat treatment details	Ac_1, K	Ac_3, K	$\Delta^\circ H^{\alpha\rightarrow\gamma}$, J g^{-1}	M_s, K	$\Delta^\circ H^{\gamma\rightarrow\alpha'}$, J g^{-1}	Solidus temperature T_s, K	Liquidus temperature T_l, K	$\Delta^\circ H_m$, J g^{-1}
1a	Plain 9Cr–1Mo quenched from 1323 K	1093	1119	17	688	42	1783	1797	230
1b	Plain 9Cr–1Mo N&T 1323 K/15 min + 1033 K/2 h	1097	1128	15	649	55	1783	1797	230
1c	Plain 9Cr–1Mo aged 823 K/500 h	1096	1107	14	671	68	1783	1797	230
1d	Plain 9Cr–1Mo aged 823 K/5000 h	1091	1111	11	679	48	1783	1797	230
1e	Plain 9Cr–1Mo aged 923 K/500 h	1087	1113	14	669	52	1783	1797	230
2	0·24 Si added 9Cr–1Mo N&T 1253 K/30 min + 1023 K/30 min	1109	1147	11	678	46	1790	1800	235
3	0·42 Si added 9Cr–1Mo N&T	1116	1114	13	663	51	1786	1799	240
4	0·6 Si added 9Cr–1Mo N&T	1130	1157	10	676	58	1775	1800	225
5a	Mod. 9Cr–1Mo N&T 1323 K/1 h + 1033 K/2 h	1125	1167	10	705	62	1775	1796	247
5b	Mod. 9Cr–1Mo N&T aged 773 K/10 000 h	1129	1165	11	721	64	1775	1796	247
5c	Mod. 9Cr–1Mo N&T aged 823 K/10 000 h	1131	1163	10	718	57	1775	1796	247
5d	Mod. 9Cr–1Mo N&T aged 873 K/10 000 h	1132	1169	10	715	60	1775	1796	247
5e	Mod. 9Cr–1Mo N&T aged 773 K/20 000 h	1129	1164	9·4	716	56	1775	1796	247
5f	Mod. 9Cr–1Mo aged 823 K/20 000 h	1128	1171	11	719	57	1775	1796	247
5g	Mod. 9Cr–1Mo N&T aged 873 K/20 000 h	1132	1172	10	709	55	1775	1796	247
6	Mod. 9Cr weld consumable 1	1028	1099	4	698	58	1793	1804	242
7	Weld consumable 2	1072	1112	16	701	51	1790	1800	240
8	Weld consumable 3	1053	1117	8	674	48	1795	1806	266
9	Weld consumable 4	1069	1107	6	677	50	1795	1806	241
10	Base metal	1094	1125	5	693	48	1793	1802	239
11a	Reduced activation steel as received Hot rolled at 1273 K + air cooled to RT	1103	1137	13	701	68	1730	1805	364
11b	Reduced activation steel 1253 K/2 h + air cooled to RT	1107	1140	11	726	73	1730	1805	364
11c	Reduced activation steel 1453 K/2 h + air cooled	1108	1131	11	753	67	1730	1805	364
11d	Reduced activation steel 1453 K/2 h + water cooled	1102	1133	12	760	74	1730	1805	364
11e	Reduced activation steel 1553 K/2 h + water cooled	1103	1143	12	731	72	1730	1805	364
11f	Reduced activation steel 1553 K + furnace cooled	1107	1142	8	735	62	1730	1805	364
11g	Reduced activation steel N&T 1253 K/air cooled + 1053 K/2 h	1097	1122	14	714	63	1730	1805	364
11h	Reduced activation steel N&T 1253 K/air cooled + 1053 K/5 h	1109	1142	13	701	66	1730	1805	364

*The quoted M_s temperature is obtained for a solutionising temperature of 1273 K and at 99 K min^{-1} cooling rate.

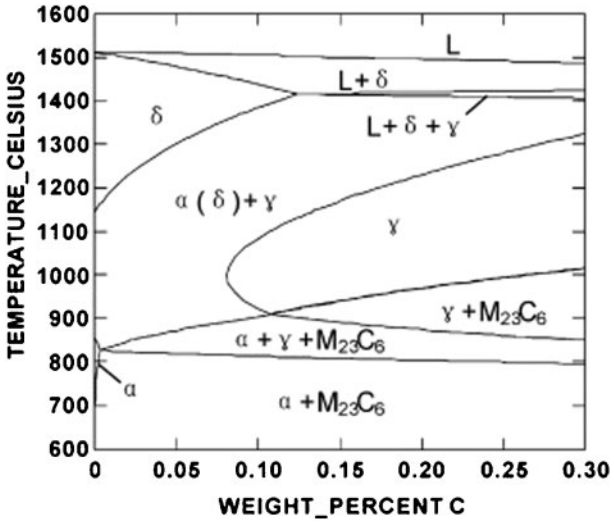

6 Calculated vertical section for high chromium ferritic steels, adopted from work of Igarashi *et al.*[42]

chromium) dissolution do also play a role in deciding the variations in Ac_3, the austenite finish temperature. Apart from the five welding consumables, which by design contain high (Ni + Mn) content, the variation in Ac_1 for the other generic 9Cr base metals follow generally an increasing pattern with the increasing chromium equivalent given by the relation

$$Cr_{eq} = [Cr] + 6[Si] + 11[V] + 5[Nb] + 2.5[Ta] + 1.5[W] - 4[Ni] - 2[Mn] - 30[N] - 40[C] \quad (1)$$

In the above relation, the concentration of each element is expressed in wt-%. Although the present experimental study samples only a very limited range in Cr equivalent, the above relation is found to hold equally good for the extensive data obtained by Finkler and Schirra as well.[43] In specific terms, it emerges from this study that an increase in the Si content of 9Cr variety from 0·24 to 0·6 wt-% for steels nos. 2–4 listed in Table 1, also increases the Ac_1 temperature. The role of silicon in affecting the relative stability of ferrite and austenite phases in high chromium steels is somewhat indirect in the sense that silicon manifests its effect by acting in conjunction with and besides modifying the influence of other solutes on carbide stability.[47] In this study, silicon is found to enhance the stability of α-ferrite and this we believe is done by retarding the dissolution kinetics of $M_{23}C_6$ carbide phase. At present, we do not have any direct experimental evidence to support this hypothesis, but it is found that silicon enhancement to a moderate level reduced the carbide coarsening kinetics in 9Cr steels.[48] In view of this, we may tentatively conclude that the major role of silicon is one of retarding the kinetics of diffusional austenitisation and thereby expand the width of the intercritical domain. The replacement of Mo and Nb on the other hand by more cohesive bcc substitutes such as W and Ta in reduced activation steel (steel no. 11 in Table 1) has again served to increase Ac_1 by a small but definite amount, as compared to say, the plain or modified 9Cr variety. The presence of W and Ta in addition, affects the carbide dissolution kinetics as they serve to reduce the effective substitutional atom mobility in the ferrite phase.[49]

Among the five modified 9Cr weld consumable compositions (steel nos. 6–10 in Table 1) investigated here, there is a clear tendency for the Ac_1 temperature to decrease with an increase in the combined (Ni + Mn) content. Thus all the weld consumables have lower Ac_1 than the corresponding base metal, a fact in conformity with the general expectation.

Effect of aging

Apart from composition, it is also known that the starting microstructure has considerable influence on the kinetics of austenitisation transformation, as for example suggested by the experiments of Caballero *et al.* on low alloy steels.[28] In the present study, the authors have conducted limited continuous heating DSC experiments on samples aged to longer times, typically of the order of 5000 h at two select temperatures, namely 823 and 873 K for plain 9Cr–1Mo steel. In addition, a few samples of modified 9Cr–1Mo variety have also been thermally aged to very long durations up to about 20 000 h at temperatures 773–873 K. It is well known, that while N&T treatment produced the tempered martensitic microstructure containing small submicron sized (about 100–200 nm) $M_{23}C_6$ and a little finer MX type precipitates, the effect of thermal aging is one of significant substructure relaxation of the tempered ferrite matrix, followed by appreciable carbide coarsening. In case of modified 9Cr steels or steels containing W, and Ta, thermal aging to very long time durations precipitates the embrittling Laves phase $(Fe,Cr)_2(Mo,W)$.[50] Thermal aging is thus accompanied by precipitation of carbides, intermetallic phases and a slight change in composition of the ferrite matrix as well as its defect density depending on time and temperature of aging.[51–54] From the data presented in Table 4, it can be observed that in the case of both plain and modified 9Cr steels, aging serves to increase the austenite start Ac_1 and finish Ac_3 temperatures. As the electron microscopy studies of Shtansky *et al.*,[32] and that of Lenel and Honeycombe[30,31] on high alloy medium carbon ferritic steels suggest, that coarser carbides take longer time to dissolve completely; and hence their effect is one of increasing the Ac_3 temperature more appreciably than Ac_1. It must also be added that this effect is more distinctly manifest under rapid heating conditions. A clear portrayal of this effect is seen in the continuous heating transformation diagram, constructed in the present study from the transformation temperature data obtained at various heating rates. One such typical continuous heating transformation diagram for 9Cr steel is shown in Fig. 7, wherein the expanding nature of the intercritical region with increasing heating rates is self-evident.

Melting temperature and enthalpy

As mentioned elsewhere here, there has not been much information in literature on the systematic variation of melting point in 9Cr steels. In view of this, an attempt has been made here to correlate the experimental values of the melting temperature T_m, with that estimated by an empirical expression of the form

$$T_m/K = 1808\{50C + 5Si + 5Mn + 5Cu + 0.7Cr + 1Ni + 0.5Mo + 0.5V + 30P + 25S\} \quad (2)$$

The above expression is an empirical modification of the one suggested earlier by Hrivnak.[55] In this relation, the concentration of each element is expressed in wt-%.

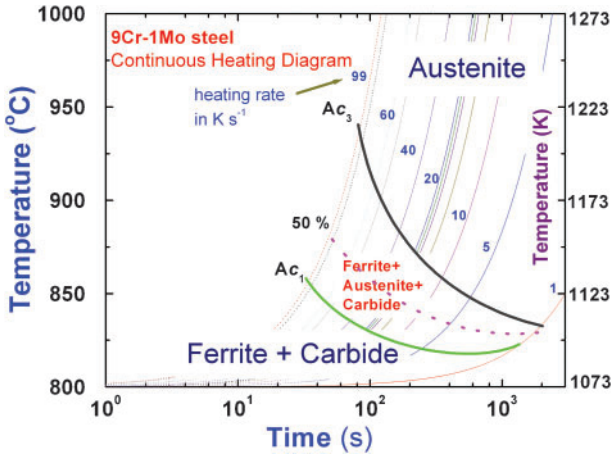

7 Typical continuous heating transformation diagram for 9Cr–1Mo steel obtained in this study. Note kinetics induced enlargement of ferrite+carbide+austenite, three phase region under fast heating conditions. Number on each curve designates heating rate in K min^{-1}

The estimated values are lower than the experimental ones by 15–20 K, and this mismatch is found to be more for the weld consumables. Nevertheless, it must be pointed out that theoretical prediction of melting temperature is a formidable task and considering this fact, the agreement between experiment and the empirical estimate given by equation (2) may be considered as quite satisfying. In Fig. 8, the experimental melting point scenario is graphically portrayed for the 9Cr steels.

As for the measured enthalpy values of on-heating α-ferrite+carbides$\rightarrow\gamma$-austenite transformation ($\Delta^{\circ}H^{\alpha\rightarrow\gamma}$) are concerned, no authentic systematics seems to emerge from the present study with respect to composition. The weld consumables containing high (Ni+Mn) content registered the lower bound values for $\Delta^{\circ}H^{\alpha\rightarrow\gamma}$, while for the rest it varied from 9 to 17 J g^{-1}. The long term aged samples in particular recorded lower values, as the $\alpha\rightarrow\gamma$ transformation in presence of coarse carbides is likely to be more incomplete at Ac_3. While the plain 9Cr–1Mo steel in the normalised condition recorded the largest value of 17 J g^{-1}, the W, Ta containing reduced activation steel in the extremely slow furnace cooled state sets the lower bound estimate of $\sim$8 J g^{-1}. While, every precaution has been taken for reliable and individual calibration for the heat flux in each run, it must be admitted that with an average sample mass of 70 mg, it is not possible to avoid certain inhomogeneity in the sample microstructure creeping in at this level. In view of this, the measured values may be taken as typical ones for this type of steel.

M_s temperature

The martensite start temperature M_s, measured in this study for various steel compositions can be satisfactorily accounted for by a modification of the empirical relation proposed by Finkler and Schirra[43] for low carbon and high chromium (8–14 wt-%) alloys. This empirical relation is:

$$M_s = 908 - 474\{C + 0.86(N - 0.15[Nb + Zr]) - 0.066Ta\} - \{(17Cr + 33Mn + 21Mo + 20Ni + 39V + 5W) - 45Mn^2 - 25Ni^2 - 100V^2 + 10Co + 20Cu\} - 47.4Si \quad (3)$$

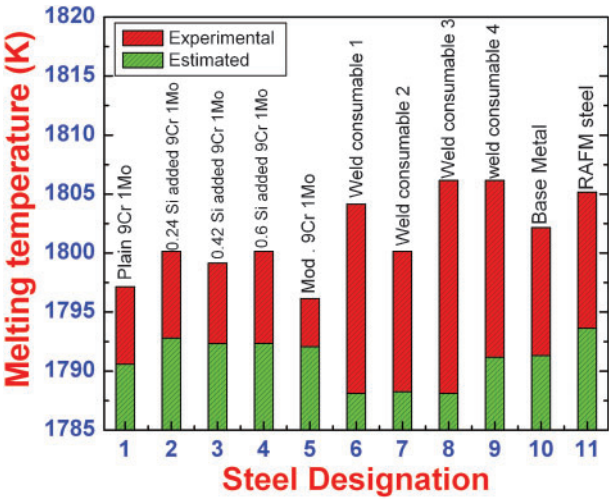

8 Comparison of observed and estimated melting points for various 9Cr steels investigated in present study

In the above relation, the concentration of different elements is expressed in wt-%. The original F–S relation did not contain non-linear contributions for Mn, Ni and V. Besides, the effect of silicon is also not included explicitly. Since the present study encompassed high (Ni+Mn) and Co containing weld consumables and also some high silicon compositions, the new nonlinear modification to F–S relation has been incorporated to empirically arrive at a predictive formula for M_s in generic 9Cr chromium steels. In Fig. 9, the measured M_s temperatures are compared against the estimated ones using equation (2) and it can be readily inferred from this graph that the agreement is fairly good. An attempt has also been made to check the predictions offered by the Bayesian neural network based regression relation suggested by Capdevila *et al.*;[56] but these predicted M_s values are not as good as the ones obtained from equation (2).

The exothermic enthalpy associated with the martensitic transformation $\Delta^{\circ}H^{\gamma\rightarrow\alpha'}$, is rather high and is found to vary from 42 to 72 J g^{-1}. The lower value is registered for plain 9Cr steel, while the larger one by W, Ta added reduced activation steel. Although, the cooling rate employed is the same for both, the austenite composition at the same solutionising temperature is

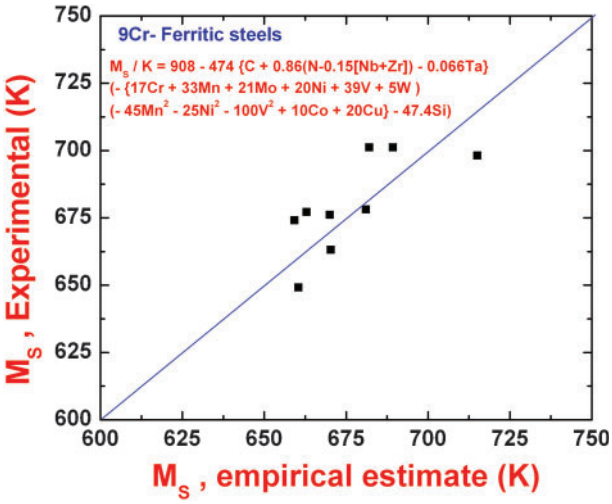

9 Comparison of experimental and estimated M_s temperature values for different 9Cr steels used in this study

different for these two steels which effectively decide the M_s as well as the latent heat associated with the martensite transformation.

One additional point that must be recalled here is the fact that the temperature and time of hold in the austenite region also decide the actual austenite composition and the size of prior austenite grain size.[56] As argued before, the extent of carbide dissolution is decided by the aforementioned two factors, which in turn affect the austenite composition considerably. Thus for example, the increase in carbon content of austenite delays the onset of martensite. Besides, the presence of any undissolved carbide particles is also likely to pin or retard the advancement of the martensite transformation front, thereby contributing to the delay in completion of martensite transformation.[57] This affects M_f, the martensite finish temperature, besides the morphology of martensite as well. The increase in austenite grain size which ensues as a result of prolonged hold at the austenitising temperature subsequent to the complete dissolution of carbides, on the other hand is known to enhance M_s.[56] Thus the martensitic transformation in high chromium steel is influenced by multiple interlinked factors. In deference to the limited scope of this study a detailed digression into the kinetic aspects of martensitic transformation is not taken up here. Nevertheless, it suffices to point out that in the temperature range 1253–1323 K, and up to a holding time of about 30 min, the M_s–M_f temperature interval remains fairly unaffected in most 9Cr steels.

In summary, it may be said that we have gathered in the present study a comprehensive dataset on transformation characteristics of many 9Cr based steel compositions. The results are consistently argued in the light of prevailing knowledge based on 9Cr steels. It is believed that these experimental findings are of use in combined thermodynamic and finite element method based simulation studies of microstructure development under various thermomechanical processing treatments.

Conclusions

1. The results of a comprehensive characterisation of the diffusional and displacive transformation temperatures and enthalpies up to the melting regime, of 10 different compositions of low carbon 9Cr steels have been presented in this study. Accurate estimates of Ac_1, Ac_3, M_s temperatures, the dissolution regions of both $M_{23}C_6$ and MX carbides, besides the melting range have been made.

2. The on-heating $\alpha \rightarrow \gamma$ transformation temperatures are found to be dependent on composition and the starting microstructure. The addition of silicon to standard 9Cr variety, Nb and V in modified 9Cr, and W, Ta in reduced activation steel, all contribute to the increase in Ac_1 through a retardation of austenitisation kinetics. The presence of enhanced (Ni + Mn) content in modified 9Cr weld consumables contributes to the decrease in Ac_1.

3. It is also found that the carbide dissolution is somewhat sluggish under fast heating conditions, which results in a kinetics mediated expansion of the inter critical region.

4. It is found that upon prolonged ageing, both Ac_1 and Ac_3 transformation temperatures exhibit a mild but definite increase, and this increase is more for the ferrite finish Ac_3 temperatures.

5. The critical cooling rate for martensite formation is found to be about 4–5 K min^{-1}. The compositional dependence of the martensite start temperature M_s, is adequately expressed by the modified Finkler–Schirra type empirical parametrisation.

6. The enthalpies of austenite formation upon heating and martensite transformation on cooling have been determined.

Acknowledgements

The authors thank Dr P. R. Vasudeva Rao, Director, Metallurgy, Materials and Chemistry group for his encouragement and sustained support during the course of this work. The various 9Cr steels including the RAFM, have come from MIDHANI, while the silicon added version from DMRL, Hyderabad. Our sincere thanks are due to these organisations for supporting IGCAR's indigenous material development initiative. Mr B. Jeya Ganesh, acknowledges, IGCAR-DAE, for the award of a senior research fellowship at IGCAR.

References

1. F. Masuyama: *ISIJ Int.,* 2001, **41**, 612–625.
2. V. K. Sikka, C. T. Ward and K. C. Thomas: Proc. on 'Ferritic steels for high-temperature applications', (ed. A. K. Khare), 65–84; 1983Metals Park, OH, ASM.
3. F. Abe, M. Igarashi, N. Fujitsuna, K. Kimura and S. Muneki: Proc. Conf. on 'Advanced heat resistant steel for power generation', San Sebastian, Spain, April 1988, Cambridge University Press, 84 –97.
4. T. Fujita: *ISIJ Int.*, 1992, **32**, 175–181.
5. W. L. Bell, T. Lauritzen and S. Vaidyanathan: Proc. Top. Conf. on 'Ferritic alloys for use in nuclear energy technologies – ferritics for breeder reactor in-core applications', (ed. J. W. Davis and D. J. Michel), 113–124; 1983, Warrendale, PA, The Metallurgical Society/AIME.
6. R. L. Klueh: *Int. Mater. Rev.*, 2005, **50**, 287–310.
7. P. J. Ennis and W. J. Quadakkers: Proc. 7th Conf. on 'Materials for advanced power engineering', Liege, Belgium, September 2002, 1131–1142; Kluwer Academic Publishers, Belgium.
8. R. K. Williams, R. S. Graves, F. J. Weaver and D. L. McElroy: 'The physical properties of 9Cr1Mo steel from 300 to 1000 K', Proc. 17th Int. Thermal Conductivity Conf., Gaithersburg, MD, USA, June 1981, 219–228; Plenum Press.
9. K. Maruyama, K. Sawada and J.-I. Koike: *ISIJ Int.,* 2001, **41**, 641–653.
10. H. Cerjak, P. Hofer and B. Schaffernak: *ISIJ Int.*, 1999, **39**, 874 – 888.
11. F. V. Ellis, J. F. Henry and B. W. Roberts: Proc. Conf. on 'New alloys for pressure vessels and piping', Vol. 201, 55–63; 1990, New York, ASME.
12. R. K. Shiue, K. C. Lan and C. Chen: *Mater. Sci. Eng. A*, 2000, **A287**, 10–16.
13. R. L. Klueh, K. Ehrlich and F. Abe: *J. Nucl. Mater.*, 1992, **191–194**, 116–124.
14. R. L. Klueh: *Curr. Opin. Solid State Mater. Sci.*, 2004, **8**, 239–250.
15. A. G. Ioltukhovsky, V. P. Kondratev, M. V. Leont'eva Smirnova, S. N. Votinov, V. K. Shamardin, A. V. Povstyanko and T. M. Bulanova: *J. Nucl. Mater.*, 1996, **233–237**, 299–304.
16. U. E. Klotz, C. Solenthaler and D. J. Uggowitzer: *Mater. Sci. Eng. A*, 2008, **A476**, 186–194.
17. R. Blum and R. W. Vanstone: Proc. 6 th Int. Conf. on 'Charles Parsons turbine conference', Dublin, Ireland, September 2003, 489–510; Maney Publishing , London, UK.
18. F. Abe: *Sci Tech. Adv. Mater.*, 2008, **9**, 1–15.
19. F. B. Pickering: 'Physical metallurgy and the design of steels'; 1978, London, Applied Science Publishers.
20. S. J. Sanderson: Proc. Int. Conf. on 'Ferritic steels for fast reactor steam generators', (ed. S. F. Pugh and E.A. Little), 120–123; 1978, London, BNES.

21. V. Foldyna, J. Purmensky and Z. Kuban: *ISIJ Int.*, 2001, **41**, S81–S85.
22. E. Gmelin and S. M. Sarge: *Thermochim. Acta*, 2000, **347**, 9–13.
23. M. J. Richardson: 'Compendium of thermophysical property measurement techniques', (ed. K. D. Maglic *et al.*), Vol. 2, 519–545; 1992, New York, Plenum Press.
24. B. Jeyaganesh, S. Raju, E. Mohandas, S. Murugesan and M. Vijayalakshmi: *Int. J. Therm. Phys.*, 2009, **30**, 619–634.
25. S. Raju, B. Jeyaganesh, A. Banerjee and E. Mohandas: *Mater. Sci. Eng. A*, 2007, **A465**, 29–37.
26. M. Tamura, H. Iida, H. Esaka and K. Shinozuka: *ISIJ Int.*, 2003, **43**, 1807–1813.
27. L. Karmazin: *Mater. Sci. Eng.*, 1988, **100**, 201–206.
28. F. G. Caballero, C. Capdevila and C. Garcia de Andres: *ISIJ Int.*, 2001, **41**, 1093 – 1102.
29. B. C. Schaffernak and H. H. Cerjak: *Calphad*, 2001, **25**, 241–251.
30. U. R. Lenel: *Scr. Metall.*, 1983, **47**, 471–474.
31. U. R. Lenel and R. W. K. Honeycombe: *Metal. Sci.*, 1984, **18**, 201–205.
32. D. V. Shtansky, K. Nakai and Y. Ohmori: *Z. Metallkd.,* 1999, **90**, 25–37.
33. V. Gaffard, A. F. Gourgues-Lorenzon and J. Besson: *ISIJ Int.*, 2005, **45**, 1915–1924.
34. R. L. Klueh: *J. Nucl. Mater.,* 2008, **378**, 159–166.
35. V. A. Yardley and Y. de Carlan: *J. Phase Eq. Diffus.*, 2006, **27**, 102–112.
36. M. Yoshino, Y. Mishima, Y. Toda, H. Kushima, K. Sawada and K. Kimura: *ISIJ Int.*, 2005, **45**, 107–115.
37. S. Raju: unpublished research.
38. T. Sourmail and C. Garcio-Mateo: *Compos. Mater. Sci.*, 2005, **34**, 323–334.
39. Y. Zhu and J. Devletian: *J. Mater. Sci.*, 1991, **26**, 6218–6222.
40. G. Ruitenberg, E. Woldt and A. K. Petford-Long: *Thermochim. Acta*, 2001, **378**, 97–105.
41. M. J. Starink: *Thermochim. Acta*, 2003, **404**, 163–176.
42. M. Igarashi, S. Muneki and F. Abe: Proc. 6th Conf. on 'Mateials for advanced power engineering', Liege, Belgium, 1998, 637–646; Kluwer Academic Publishers, Belgium.
43. H. Finkler and M. Schirra: *Steel Res.*, 1996, **67**, 328–342.
44. H. Naoi and T. Fujita: Proc. on 'New steels for advanced plant up to 620°C', (ed. E. Metcalfe); 1995, Oxon, PICA Publ. Services.
45. C. Berger: Proc. on 'High temperature materials for power engineering', (ed. D. Coutsouradis *et al.*), 47–72; 1994, Dordrecht, Kluwer Academic Publishers.
46. A. Danon and A. Alamo: *J. Nucl. Mater.*, 2001, **307–311**, 479–483.
47. L. Gavard, H. K. D. H. Bhadeshia, D. J. C. MacKay and S. Suzuki: *Mater. Sci. Technol.*, 1996, **12**, 453–463.
48. Y. Y. Fin and R. G. Faulkner: *Mater. Sci. Eng. A*, 2003, **A344**, 92–102.
49. J. Cermak, J. Ruzickova and A. Pokorna: *Scr. Metall. Mater.*, 1995, **32**, 1631–1635.
50. Y. Murata, M. Kamiya, T. Kuneida, A. M. Abdel-Daiem, T. Koyama, M. Morinaga and R. Hashizume: *ISIJ Int.*, 2005, **45**, 101–105.
51. J. M. Vitek and R. L. Klueh: *Metall. Trans. A*, 1983, **14A**, 1047–1058.
52. M. Tamura, Y. Haruguchi, M. Yamashita, Y. Nagaoka, K. Ohinata, K. Ohnishi, E. Iitoh, H. Ito, K. Shinozuka and H. Esaka: *ISIJ Int.*, 2006, **46**, 1693–1702.
53. J. D. Robson and H. K. D. H. Bhadeshia: *Calphad*, 1996, **20**, 447–460.
54. A. Bjarbo and M. Hattestrand: *Metall. Trans. A*, 2001, **32A**, 20–27.
55. I. Hrivnak: *ISIJ Int.*, 1995, **35**, 1148–1156.
56. C. Capdevila, F. G. Caballero and C. Garcia de Andres: *ISIJ Int.*, 2002, **42**, 894–902.
57. S. Raju, B. Jeyaganesh, A. K. Rai and E. Mohandas: Unpublished Research, 2009.